Multi-parametric flutter analysis of a morphing wing trailing edge

R. Pecora
rosario.pecora@unina.it
M. Magnifico, F. Amoroso and E. Monaco
University of Naples, 'Federico II'x
Department of Aerospace Engineering
Napoli
Italy

ABSTRACT

The development of adaptive morphing wings has been individuated as one of the crucial topics in the greening of the next generation air transport. Research programs are currently running worldwide to exploit the potentiality of morphing concepts in the optimisation of aircraft efficiency and in the consequent reduction of fuel burn. Among these, SARISTU represents the largest European funded research project which ambitiously addresses the challenges posed by the physical integration of smart concepts in real aircraft structures; for the first time ever, SARISTU will experimentally demonstrate the structural feasibility of individual morphing concepts concerning the leading edge, the trailing edge and the winglet on a full-size outer wing belonging to a CS-25 category aircraft. In such framework, the authors intensively worked on the definition of aeroelastically stable configurations for a morphing wing trailing edge driven by conventional electromechanical actuators. Trade off aeroelastic analyses were performed in compliance with CS-25 airworthiness requirements (paragraph 25.629, parts (a) and (b)-(1)) in

Paper No. 4041. Manuscript received 23 July 2013, accepted 20 May 2014.

https://doi.org/10.1017/S000192400000974X Published online by Cambridge University Press

order to define safety ranges for trailing-edge inertial and stiffness distributions as well as for its control harmonics. Rational approaches were implemented in order to simulate the effects induced by variations of trailing-edge actuators' stiffness on the aeroelastic behaviour of the wing also in correspondence of different dynamic properties of the trailing-edge component. Reliable aeroelastic models and advanced computational strategies were properly implemented to enable fast flutter analyses covering several configuration cases in terms of structural system parameters. Already available finite elements models were processed in MSC-NASTRAN® environment to evaluate stiffness and inertial distributions suitable for the stick-equivalent idealisation of the reference structure. A parametric stick-equivalent model of the reference structure was then generated in SANDY3.0, an in-house developed code, that was used for the definition of the coupled aero-structural model as well as for the solution of aeroelastic stability equations by means of theoretical modes association in frequency domain.

Obtained results were finally arranged in stability carpet plots efficiently conceived to provide guidelines for the preliminary design of the morphing trailing-edge structure and therein embedded actuators.

NOMENCLATURE

A/C	aircraft
AIC	Aerodynamic Influence Coefficients
BMX	Bending Moment about *X*-axis
BMZ	Bending Moment about *Z*-axis
CONM2	Concentrated (lumped) mass element[20]
DMIG	Direct Matrix Input at Grids[20]
EA	stiffness to normal force
EI_{max}	maximum bending stiffness
EI_{min}	minimum bending stiffness
f	frequency
FE	Finite Element
FY	force acting along *Y*-axis
GJ	torsional stiffness
k_a	locked actuator (torsional) stiffness
MT	torque
RBE2	2 nodes rigid body element[20]
RY	rotation around *Y*-axis
RZ	rotation around *Z*-axis
TY	displacement along *Y*-axis
TZ	displacement along *Z*-axis
V_D	dive speed
λ	$= \lvert TZ/RY \rvert$

INTRODUCTION

Aircraft wings are usually optimised for a specific design point. However, since they operate in a wide variety of flight regimes, some of these have conflicting impacts on aircraft design, as an aerodynamically efficient configuration in one instance may perform poorly in others.

https://doi.org/10.1017/S000192400000974X Published online by Cambridge University Press

Ideally rigid, non-deformable wing structures preclude any adaptation to changing conditions; moreover, conventional devices, such as flaps or slats, lead to limited changes of the overall shape with narrow benefits compared with those that could be obtained from a wing structure that is inherently deformable and adaptable[1].

Several adaptive wings concepts of varying complexity may be found in literature with regard to specific applications and objectives: from variable camber flaps conceived to optimise take-off and landing performances[2,3], to wings provided with twist angle variation[4] or overall camber-morphing capabilities[5-9] enabling aerodynamic flow control and drag reduction, from variable chord wing segments[10], to variable aspect ratio wings[11] for planform control during aircraft mission. Year by year, new aspects are being investigated[12], thus confirming a positive trend in the exploration of the wing morphing topic. It is therefore not surprising that in the last decades several research programs were launched worldwide to exploit the potentials of morphing concepts, especially for what concerns the optimisation of aircraft efficiency and the consequent reduction of fuel consumption[13]; among these, SARISTU[14] represents the largest European funded research project which ambitiously addresses the challenges posed by the physical integration of smart concepts in real aircraft structures; for the first time ever, SARISTU will experimentally demonstrate the structural feasibility of individual morphing concepts on a full-size outer wing belonging to a CS-25 category aircraft. In the framework of SARISTU project, research is carried out to develop an adaptive trailing-edge device aiming at maximising wing aerodynamic performance in cruise condition. The shape of wing trailing-edge camber is controlled during flight in order to compensate the weight reduction following the fuel burning, by allowing the trimmed configuration to remain optimal in terms of efficiency (lift to drag ratio) or minimal drag. Trailing-edge adaptations were investigated to achieve significant benefits in aircraft fuel consumption whose reduction ranges from 3% to 5% depending on flight mission. Target morphed shapes to be reproduced in flight were determined through CFD-based optimisations analyses; the same applies to the overall dimensions of the morph-able trailing edge (chord/span, see Fig. 1).

A novel smart structure was investigated to enable the controlled modification of the trailing-edge shape. The concept developed to produce wing camber variations is based on segmented adaptive ribs. They consist of finger-like segments covered by a highly flexible skin. Single-degree-of-freedom mechanisms, driven by load-bearing electro-mechanical actuators, are then used to change the wing camber by controlling the adaptive ribs individually[15-16]. This solution offers

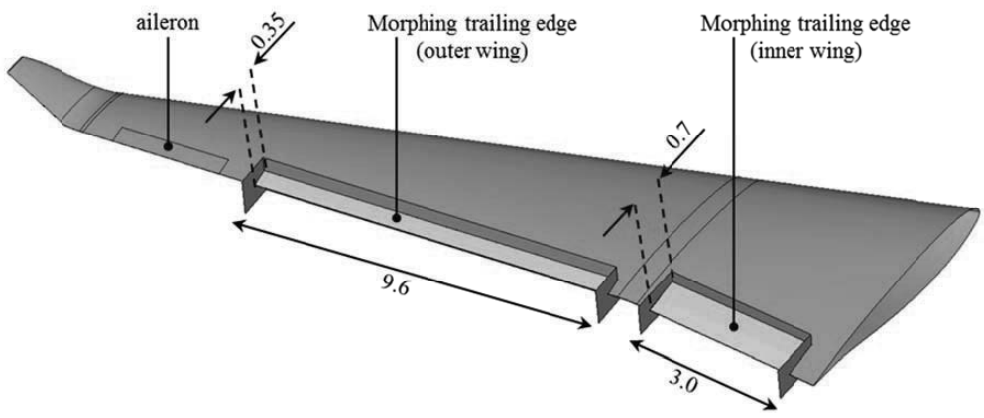


Figure 1. Morphing trailing edge overall dimensions (metres).

https://doi.org/10.1017/S000192400000974X Published online by Cambridge University Press

remarkable advantages with respect to compliant structures regarding both actuation energy and weight. Furthermore, its aerodynamic superiority over traditional hinged flaps was preliminarily proven. On the other hand, the presence of a large and unconventional movable device carrying significant aerodynamic loads resulted in a more complex wing system and therefore in a pretty challenging design especially for what regards aeroelastic stability issues. The impact of the morphing trailing edge on the aeroelastic behaviour of the wing was then considered since the preliminary design phase of the morphing device. Trade-off flutter analyses were performed to properly define safety ranges for trailing-edge inertial and stiffness distributions, as well as for control line harmonics, assuring overall system compliance with CS-25 airworthiness requirements, paragraph 25.369 (a) and (b)-(1) (absence of any aeroelastic instability up to 1·15 times the aircraft dive speed[17]. Rational approaches were implemented in order to simulate the effects induced by variations of trailing-edge actuators' stiffness on the aeroelastic behaviour of the wing, also in correspondence of different dynamic properties of the trailing-edge structure. Already available finite elements models were processed in MSC-NASTRAN® environment to evaluate stiffness and inertial distributions suitable for the stick-equivalent idealisation of the reference structure. A parametric stick-equivalent model of the reference structure was then generated in SANDY3.0, an in-house developed code, that was used for the definition of the coupled aero-structural model as well as for the solution of aeroelastic stability equations by means of theoretical modes association in frequency domain.

Adopted methodologies and obtained results have been outlined in the following paragraphs; for completeness sake, a general description of SANDY 3.0 software has been provided as appendix of this paper.

2.0 AEROELASTIC MODEL GENERATION

2.1 Structural model

In order to perform fast sensitivity analyses, a simplified and fairly representative structural model of the wing system was generated referring to a stick-equivalent representation[18].

Stiffness and inertial properties of the aeroelastic model were extracted by working on two FE models that were elaborated by concurring partners of SARISTU Consortium to provide adequate data on reference wing structure:

Model A : FE model of the right wing box structure, tailored for the preliminary assessment of wing's dynamic and aeroelastic behaviour (Fig. 2(a));

Model B : FE model of the right wing structure, covering also leading and (conventional) trailing-edge architectures and characterised by refined mesh specifically conceived for detailed stress analyses (Fig. 2(b)).

The wing box mesh of Model A was generated according to the idealisation process typically adopted for single-cell thin-walled wing sections[19]: shell elements were used to model skin panels as well as ribs and spars' webs, while bar elements were adopted for stringers and spar caps. A two-spar configuration with 31 ribs (20 along the wing, 6 along the winglet) and 5 stringers on both upper and lower skin panels was referred to.

The mesh size of spars' webs surfaces was defined congruently with the location of ribs; in other terms, for the generic wing-box bay delimited by two consecutive ribs, each spar web was simulated by means of a single shell element. The same mesh size was adopted for spar caps and stringers thus leading to one single bar element for each of these items along each bay of the wing box (Fig. 3).

https://doi.org/10.1017/S000192400000974X Published online by Cambridge University Press

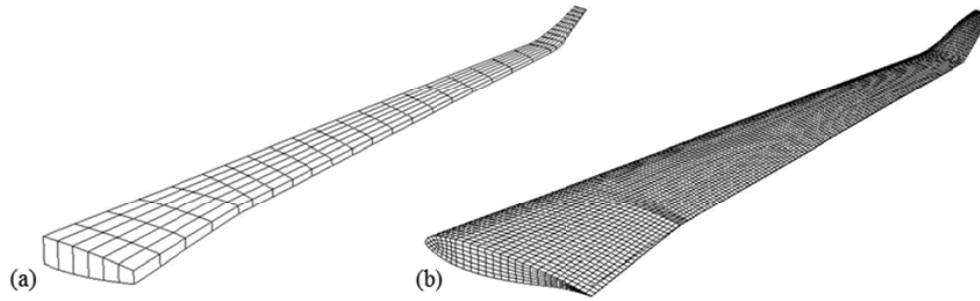


Figure 2. FE reference models: (a) Model A, (b) Model B.

The mesh of the upper and lower skin surfaces was sized along the span according to ribs location and along the chord according to stringers and spars' caps positions. For the generic wing-box bay, both upper and lower skin panels resulted therefore modelled through six shell elements along the chord.

For congruency and consistency sake, ribs' mesh followed the discretisation adopted for skin panels thus leading to 6 shell elements for each rib panel.

Model B was obtained from Model A by increasing the mesh size for local stress analyses purpose. Elements properties† along wing and winglet boxes were preserved, while new shell elements were added to simulate leading and (conventional) trailing-edges structural behaviour.

The position of wing box elastic axis was evaluated by means of an iterative procedure consisting of seven main steps:

1. A trial position of the elastic axis was assumed;
2. Nodes were added to Model A in correspondence of the intersection points between the elastic axis and ribs' planes;
3. At each rib, RBE2 elements[20] were generated to slave the nodes of the rib boundary to the node at the intersection between the rib plane and the (imposed) elastic axis;
4. An arbitrary torque *MT*, was applied along the elastic axis and in correspondence of its intersection with the plane of the rib located at wing tip. The master node on the rib plane at the wing root was constrained in all degrees of freedom;

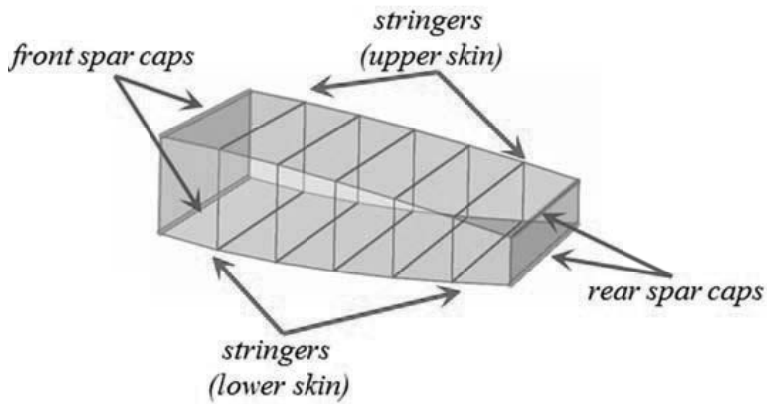


Figure 3. Mesh of wing box bay (Model A) :bar elements (blue and red), shell elements (grey, transparent).

† Element properties details (e.g. shell elements thickness, bar elements sections, materials data) are intentionally not reported since they are strictly confidential.

https://doi.org/10.1017/S000192400000974X Published online by Cambridge University Press

5. Static analysis was performed in MSC-NASTRAN® environment and the following displacements were evaluated:

   TZ_i: displacement of the master node on the i-th rib along the axis Z perpendicular to the elastic axis and to the wing box middle plane (vertical bending displacement induced by MT);

   RY_i: rotation of the master node on the i-th rib around the axis Y coincident with elastic axis (torsion induced by MT);

6. Ratios $\lambda_i = |TZ_i/RY_i|$ were evaluated at each rib location thus providing the offset of the actual shear centre with respect to its supposed position;
7. At each rib location,. the master node defined at point 3 was shifted chordwise by the amount λ_i;
8. Steps from 4 to 7 were repeated until all ratios λ_i resulted quite equal to zero.

The same procedure was followed for the determination of the winglet elastic axis.

Stiffness distributions along the span of the wing box (/winglet box) equivalent beam were determined with reference to the Model A (modified according to the actions described at points 2 and 3) and to the following equations:

$$GJ(y) = \frac{MT}{\frac{\mathrm{d}}{\mathrm{d}y}[RY(y)]} \quad \ldots (1)$$

$$EI_{\min}(y) = \frac{BMX}{\frac{\mathrm{d}}{\mathrm{d}y}[RX(y)]} \quad \ldots (2)$$

$$EI_{\max}(y) = \frac{BMZ}{\frac{\mathrm{d}}{\mathrm{d}y}[RZ(y)]} \quad \ldots (3)$$

$$EA_{\max}(y) = \frac{FY}{\frac{\mathrm{d}}{\mathrm{d}y}[TY(y)]} \quad \ldots (4)$$

where:

- X,Y,Z are the axis of a Cartesian reference system characterised by:
  - origin at the root of the wing box (/winglet box) elastic axis (at the inner rib location of the item);
  - Y axis coincident with the item elastic axis and positively oriented towards item's tip;
  - XY plane coincident with wing (/winglet) middle surface;
  - Z axis normal to XY plane and upwards oriented.
- y is the generic coordinate along the Y-axis.
- $GJ(y)$ is the torsional stiffness distribution.
- $EI_{min}(y)$ is the vertical bending stiffness distribution (stiffness to bending across XY plane).

https://doi.org/10.1017/S000192400000974X Published online by Cambridge University Press

- $EI_{max}(y)$ is the lateral (fore and aft) bending stiffness distribution (stiffness to bending across *YZ* plane).
- $EA(y)$ is the distribution of the stiffness exhibited with respect to forces acting along the elastic axis (normal-to-sections solicitations).
- *MT* and $RY(y)$ are respectively an arbitrary torque moment acting around the elastic axis (*Y*-axis) at its free-end and $RY(y)$ is the rotation around the *Y*-axis of the cross section at spanwise location *y*.
- *BMX* and $RX(y)$ are respectively an arbitrary bending moment acting around *X*-axis at elastic axis free-end and $RX(y)$ is the rotation around the *X*-axis of the cross section at spanwise location *y*.
- *BMZ* and $RZ(y)$ are respectively an arbitrary bending moment acting around *Z*-axis at elastic axis free-end and $RZ(y)$ is the rotation around the *Z*-axis of the cross section at spanwise location *y*.
- *FY* and $TY(y)$ are respectively an arbitrary force acting along elastic axis (*Y*-axis) at its free-end and $TY(y)$ is the displacement along the *Y*-axis of the cross section at spanwise location *y*.

For aeroelastic stability analyses, the morphing trailing edge was modelled as a conventional movable surface characterised by an hinge line located at:

- 85% of the wing chord for the inner wing region (see Fig. 1);
- 88% of the wing chord for the outer wing region (see Fig. 1).

Stiffness properties of the equivalent beams representing the hinge lines were obtained always by Equations (1)-(4) but referring, in this case, to Model B.

The stiffness distributions of all the other structural items (namely: leading edge, not movable trailing-edge portions) were considered negligible.

The effect of such items on wing aeroelastic behaviour was then considered only from the inertial standpoint (Fig. 4).

Equivalent lumped mass (/inertia) distributions were evaluated for all the structural items of the wing[18]. For the generic item, the inertial properties of each bay were evaluated on the base of

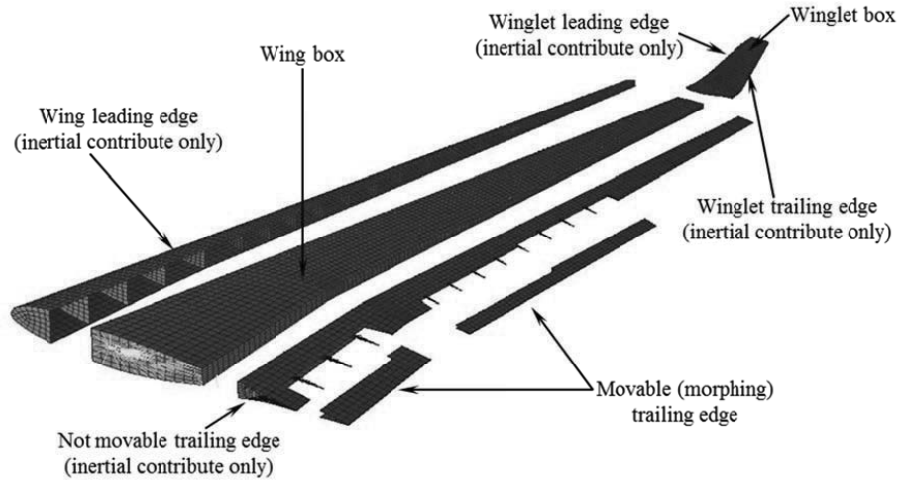


Figure 4. Items considered for the generation of the wing aeroelastic model.

https://doi.org/10.1017/S000192400000974X Published online by Cambridge University Press

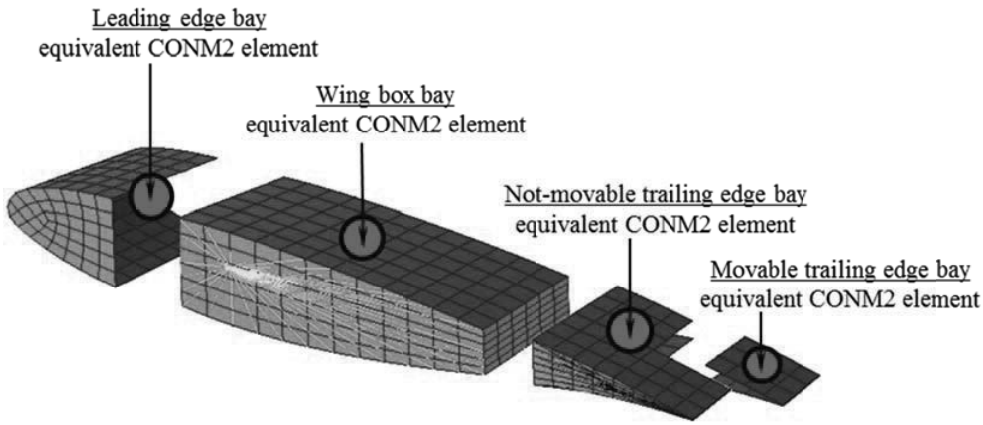


Figure 5. Example of inertial condensation for a wing bay.

finite elements model data; such properties were then assigned to a CONM2 element[20] located at the centre of gravity of the bay (Fig. 5).

Model A was used to evaluate the inertial properties of the bays belonging to wing and winglet box, while Model B was used for leading and trailing-edge bays.

CONM2 elements were rigidly connected to the closest grid of the beam-equivalent model of the pertaining item.

The structural model of the left wing was obtained by mirroring with respect to aircraft symmetry plane. Right and left hand side models were then linked to a central node (on aircraft symmetry plane) by means of DMIG elements[20] generated to simulate the stiffness of the wing-fuselage interface (Fig. 6). A CONM2 element lumping mass and plunge inertia of the aircraft body was placed on the central node. The hinge lines of the morphing trailing edge were linked to the elastic axis of the wing by means of beam elements; pin flags[20] were properly imposed at the end-nodes of such elements to release the rotation around the hinge lines. A torsional spring element was finally added at the inner node of each hinge line to simulate actuators stiffness.

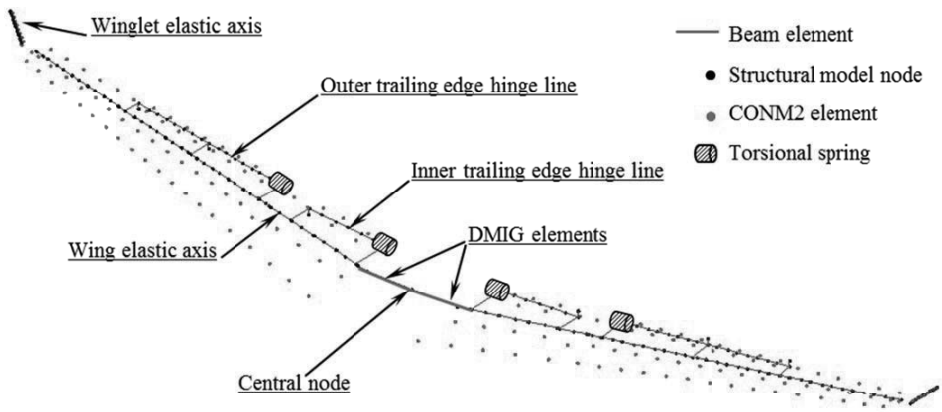


Figure 6. Equivalent structural model of the wing (rigid elements hidden for clarity).

https://doi.org/10.1017/S000192400000974X Published online by Cambridge University Press

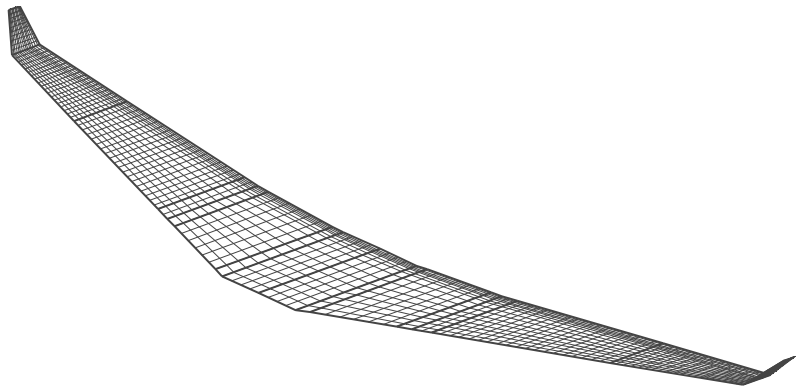


Figure 7. Aerodynamic model (thick lines represents panels' boundaries).

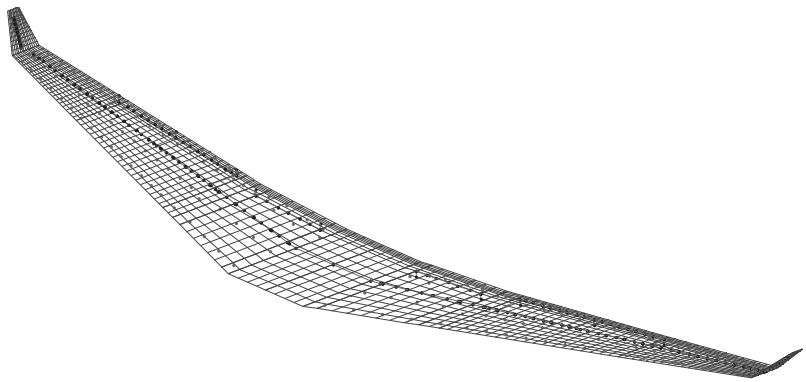


Figure 8. Structural and aerodynamic models.

2.2 Aerodynamic and interpolation model

Matrices of unsteady aerodynamic influence coefficients (AIC[21]) were evaluated by means of doublet lattice method (DLM[21]). The aerodynamic lattice of the wing (Fig. 7) was generated by properly meshing the middle wing plane through 8 macro-panels for each side of the wing; macro-panels were further meshed into elementary boxes; higher boxes density was considered for the movable trailing edge and, to assure mesh uniformity also for the not-movable trailing edge. Modal displacements at the centre of each aerodynamic box were obtained by means of linear spline functions[21] attached to support-nodes of the structural model. In Fig. 8 the aerodynamic and structural models have been depicted together.

3.0 TRADE-OFF FLUTTER ANALYSIS

3.1 Assumptions and investigation cases

Flutter analyses were carried out under the following assumptions:

- PK-continuation method with rationalisation of generalised aerodynamic forces[21] for the evaluation of modal frequencies and damping trends versus flight speed;

https://doi.org/10.1017/S000192400000974X Published online by Cambridge University Press

- theoretical elastic modes association in the frequency range 0Hz-60Hz (elastic modes being pertinent to free-free aircraft, with only plunge and roll motions allowed);
- modal damping (conservatively) equal to 0·01 for all the elastic modes;
- sea-level altitude, flight speed range 0-300ms^{-1} (≈1·5 V_D†, $V_D \approx 200$ms^{-1}).

Flutter speeds were evaluated in correspondence of different settings for the movable trailing edge, each setting being defined by means of three (trade-off) parameters:

- inertial distribution;
- stiffness distribution;
- harmonic frequency (i.e. frequency of the elastic deflection at locked actuators).

Investigated cases mapped three different inertial distributions in combination with three different stiffness distributions and five harmonic frequencies of the movable surface (Table 1); the trade-off domain was therefore composed by forty-five different configurations of the movable trailing edge.

The harmonic frequency was set by manipulating the stiffness of the torsional spring used to simulate movable trailing-edge actuators (see paragraph 2.1); in order to get a given frequency f, the torsional stiffness K_a of the actuators was imposed equal to:

$$K_a = I(2\pi f)^2 \quad \ldots (5)$$

where I stands for the inertia of the movable trailing edge around its hinge line.

The condition $f = 0$Hz was taken in account to simulate actuators failure; in such a case the movable trailing-edge harmonic obviously coincides with its fundamental (free rotation around the hinge line).

3.2 Summary of results

For each investigation case flutter speeds and flutter mode were evaluated. Accurate analysis of modes participation factors into flutter mode were performed in order to isolate the principal modes involved in each detected flutter.

Two types of flutter were identified for all investigated cases:

1. bell-shaped flutter
2. sharp flutter

Both flutter types occurred in all investigated cases but at different speeds; in some cases the flutter speeds related to one or to both flutter types resulted outside the speed investigation range (0:300ms^{-1}), see paragraph 3.1).

Table 1
Values of trade-off parameters

Movable trailing-edge inertial distribution	Movable trailing-edge stiffness distributions	Movable trailing-edge harmonic frequency (Hz)
Baseline	Baseline	0
Baseline*1·3	Baseline*1·15	15
Baseline*1·6	Baseline*0·85	30
		45
		60

† V_D indicates the dive speed of the aircraft. The exact value of the dive speed is confidential.

https://doi.org/10.1017/S000192400000974X Published online by Cambridge University Press

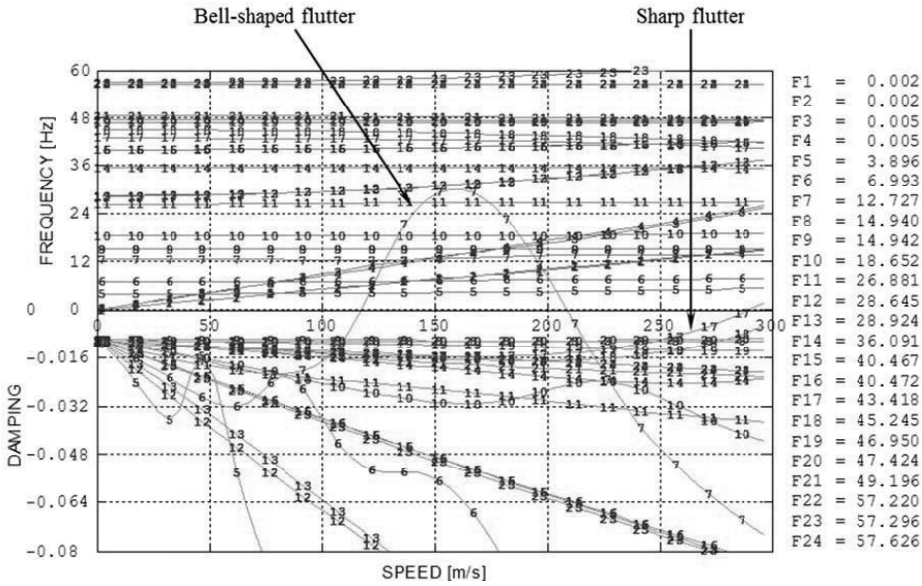


Figure 9. Modes frequency/damping versus flight speed.

In Fig. 9 the trends of modes frequencies and damping versus flight speed have been plotted with reference to a generic case of investigation for which both flutter types are present in the speed investigation range.

The first type of flutter was found to be due mainly to the coupling of two modes (binary flutter): the first symmetric wing bending (Fig. 10) and the outer trailing-edge symmetric harmonic (or fundamental, in case of actuators failure (Fig. 11).

The dynamics of the sharp flutter resulted instead more complex: three modes are mainly involved, namely, first symmetric wing bending, outer trailing-edge symmetric harmonic and outer wing symmetric torsion (Fig. 12).

A stability carpet plot was generated to provide a thorough overview of flutter speed trends versus the frequency of movable trailing-edge harmonics (Fig. 13).

Each curve of the carpet plot has been coloured according to the flutter mode it refers to; moreover the line-style of each curve has been chosen according to the pertaining trailing-edge configuration (i.e. investigation case).

Only five of the forty-five investigation cases are covered by the carpet plot; this is due to the fact that the remaining forty cases resulted in flutter speed greater than 300ms^{-1}.

The red horizontal line at constant speed equal to $1{\cdot}15V_D$, divides the carpet plot in two different regions:

- the region above the red line, defining the safe domain for flutter speed according to CS-25, paragraph 629[17];
- the region below the red line, defining the unsafe domain for flutter speed occurrence.

If the inertial distribution of the movable trailing edge is kept equal to its nominal value and its stiffness distributions is reduced by the 15%, flutter occurs at flight speeds lower than $1{\cdot}15V_D$ whatever is the frequency of the trailing-edge harmonic. The same happens if the inertial distri-

https://doi.org/10.1017/S000192400000974X Published online by Cambridge University Press

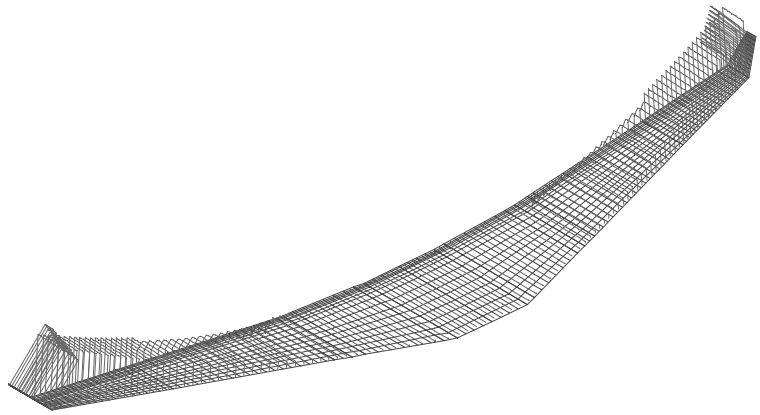


Figure 10. 1st wing bending (symmetric).

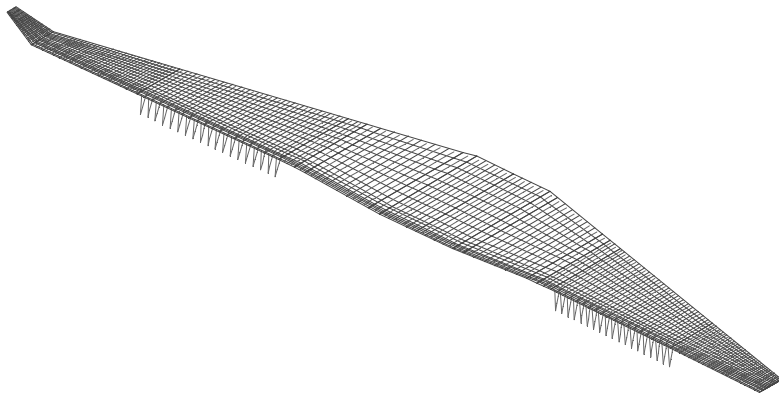


Figure 11. Outer trailing-edge harmonic (symmetric).

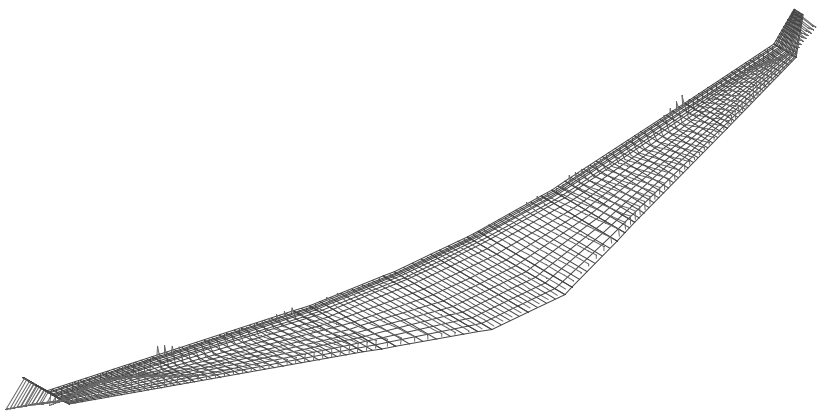


Figure 12. Outer wing torsion (symmetric).

https://doi.org/10.1017/S000192400000974X Published online by Cambridge University Press

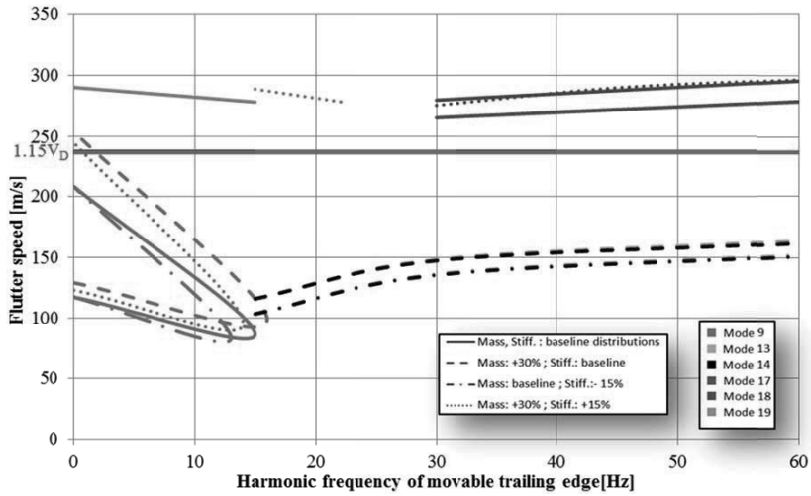


Figure 13. Carpet plot of flutter speeds.

bution is increased by the 30% and the stiffness distributions are equal to the nominal ones. These dangerous combinations of inertial and stiffness distributions are however quite unlikely to occur, since stiffness increase generally implies mass increase.

For all the other inertial/stiffness configurations covered by the carpet plot, a minimum frequency of 18Hz for the trailing-edge harmonic is sufficient to avoid any flutter instability up to $1{\cdot}15V_D$. In case of actuators failure (harmonic frequency equal to 0Hz) flutter always occurs at speeds within the certification envelope. Although the simultaneous failure of all actuators represents an event of extremely remote probability, it was found that, even in such case, flutter may be avoided by a suitable mass-balancing of the movable trailing edge.

CONCLUSIONS

The design (and validation) of a morphing trailing-edge architecture for a CS-25 category aircraft is one of the major challenges of SARISTU project. Due to the higher complexity of the system with respect to conventional solutions based on hinged flaps, it was believed necessary to take in account aeroelastic issues since the preliminary design phase of the device. To this aim trade off flutter analyses were performed in compliance with CS-25 airworthiness requirements in order to define safety ranges for trailing-edge inertial and stiffness distributions as well as for the harmonics of trailing edge's control lines. Rational approaches were therefore implemented in order to simulate the effects induced by variations of trailing-edge actuators' stiffness on the aeroelastic behaviour of the wing also in correspondence of different dynamic properties of the trailing-edge component. Reliable aeroelastic models and advanced computational strategies were properly implemented to enable fast flutter analyses covering several configuration cases in terms of structural system parameters.

Already available finite elements models were processed in MSC-NASTRAN® environment to evaluate stiffness and inertial distributions suitable for the stick-equivalent idealisation of the reference structure. A parametric stick-equivalent model of the reference structure was then generated in SANDY3.0, an in-house developed code, that was used for the definition of the

https://doi.org/10.1017/S000192400000974X Published online by Cambridge University Press

coupled aero-structural model as well as for the solution of aeroelastic stability equations by means of theoretical modes association in frequency domain.

Obtained results showed that for the most practical combinations of trailing-edge stiffness and inertial distributions, flutter is avoided if sufficient stiffness is provided by the actuation chain. On the other hand, also in the extremely remote event of simultaneous failure of all the actuators, a proper mass-balancing of the trailing edge assures the absence of any flutter instability within the certification envelope.

Such results may be regarded as general guidelines to be properly taken in account for the advanced design of the trailing-edge structure as well as for the definition of the actuation chain (actuators and control lines); flutter-free configurations resulting from trade-off analyses, represent then a well-defined reference database specifically conceived to monitor the impacts of specific design solutions on the aeroelastic stability of the wing. In the light of this consideration, the simplifications made to define trailing-edge structural models as well as actuation system elasticity, result fully compliant with

the targets of a preliminary aeroelastic investigation mainly devoted to define macro-requirements at global system level.

On the other hand, after the full definition of the morphing trailing-edge architecture, further flutter-analysis are expected to be carried out while referring to more refined structural configurations of the morphing trailing edge and therein embedded control lines; moreover, as prescribed by CS-25 requirements, several flight altitudes and aircraft mass configurations need to be explored also in combination with imposed nonlinearities in the actuation system, thus properly simulating the effects of free-plays and/or actuators jamming. These advanced analyses will however play the role of a final check for the assessed layout of the morphing system, provided that no relevant issues are envisaged whereas the design assessment will comply with the general recommendations resulting from the parametric studies reported in this work.

ACKNOWLEDGEMENTS

The research leading to these results has gratefully received funding from the European Union Seventh Framework Programme (FP7/2007- 2013) under Grant Agreement no 284562.

The authors would like to thank all SARISTU partners involved in the design of the morphing trailing-edge device.

REFERENCES

1. BARBARINO, S., BILGEN, O., AJAJ, R.M., FRISWELL, M.I. and INMAN, D.J. A review of morphing aircraft, *J Intelligent Material Systems and Structures*, 2011, **22**, pp 823–877.
2. MONNER, H.P., BEIN, T., HANSELKA, H. and BREITBACH, E. Design Aspects of the Adaptive Wing – The Elastic Trailing Edge and the Local Spoiler Bump, Proceedings of Royal Aeronautical Society Symposium on Multidisciplinary Design and Optimization, Royal Aeronautical Society Publishing, London, UK, 1998, pp 15.1–15.9.
3. PECORA, R., BARBARINO, S., CONCILIO, A., LECCE, L. and RUSSO, S. Design and functional test of a morphing high-lift device for a regional aircraft, *J Intelligent Material Systems and Structures*, 2011, **22**, (10), pp 1005–1023.
4. PECORA, R., AMOROSO, F. and LECCE, L. Effectiveness of wing twist morphing in roll control, *J Aircr*, 2012, **49**, issue 6, pp 1666-1674.
5. BARBARINO, S., PECORA, R., LECCE, L., CONCILIO, A., AMEDURI, S. and DE ROSA, L. Airfoil structural morphing based on s.m.a. actuator series: numerical and experimental results, *J Intelligent Material Systems and Structures*, 2011, **22**, pp 987–1004.
6. STANEWSKY, E. Adaptive wing and flow control technology, *Progress in Aerospace Sciences*, 2001, **37**, (7), pp 583–667.

https://doi.org/10.1017/S000192400000974X Published online by Cambridge University Press

7. BROWMAN, J., SANDERS, B. and WEISSHAAR, T. Evaluating the Impact of Morphing Technologies on Aircraft Performance, Proceedings of the Forty-Third AIAA Conference on Structures, Structural Dynamics and Materials, AIAA Paper 2002-1631, April 2002.
8. SZODRUCH, J. and HILBIG, R. Variable wing camber for transport aircraft, *Progress in Aerospace Science*, 1988, **25**, (3), pp 297–328.
9. MUNDAY, D. and JACOB, J. Active Control of Separation on a Wing with Conformal Camber, Proceedings of the Thirty-Ninth AIAA Aerospace Science Meeting and Exhibit, AIAA Paper 2001-293, January 2001.
10. PERKINS, D.A., REED, J.L. and HAVENS, E. Morphing Wing Structures for Loitering Air Vehicles, Proceedings of the Forty-Fifth AIAA Confrence on Structures, Structural Dynamics and Materials, AIAA Paper 2004-1888, April 2004.
11. BLONDEAU, J. and PINES, D. Pneumatic Morphing Aspect Ratio Wing, Proceedings of the Forty-Fifth AIAA Conference on Structures, Structural Dynamics and Materials, AIAA Paper 2004-1808, April 2004.
12. COURCHESNE, S., POPOV, A.-V. and BOTEZ, R.M. New aeroelastic studies for a morphing wing, *INCAS Bulletin*, 2012, **4**, (2), pp 19-28.
(13) BOTEZ, R.M., MOLARET, P. and LAURENDEAU, E. Laminar Flow Control on a Research Wing Project Presentation Covering a Three Year Period, Canadian Aeronautics and Space Institute (CASI) Aircraft Design and Development Symposium, Toronto, Canada, April 2007.
14. www.saristu.eu (web site of the SARISTU project)
15. DIMINO, I., CONCILIO, A., SCHUELLER, M. and GRATIAS, A. An adaptive control system for wing TE shape control, Proceedings of SPIE 8690, Industrial and Commercial Applications of Smart Structures Technologies, March 2013 (DOI: 10.1117/12.2012187).
16. DIMINO, I., SCHUELLER, M., GRATIAS, A. and FLAUTO, D. Adaptive Shape Control Architecture for Morphing Wings, Proceedings of the 6th ECCOMAS thematic Conference on Smart Structures and Materials (SMART 2013), June 2013.
17. European Aviation Safety Agency, Certification Specifications and Acceptable Means of Compliance for Large Aeroplanes – CS-25, Amendment 11 July 2011.
18. BISPLINGHOFF, R.L., ASHLEY, H. and HALFMAN, R.L. *Aeroelasticity*, Dover Publications., New York, USA, 1996
19. MEGSON, T.H.G. *Aircraft Structures for Engineering Students*, Butterworth-Heinemann, Burlington (MA), 2003, 3rd ed.
20. MSCMDNASTRAN®, Software Package, Ver. R3-2006, Reference Manual.
21. BROADBENT, E.G. Flutter and Response Calculations in Practice, *AGARD Manual on Aeroelasticity*, **3**, NASA, February 1963.
22. PECORA, R., PECORA, M. and LECCE, L. Flutter Certification of SKYCAR Aircraft: Rational Analysis and Flight Tests, Proceedings of the 3rd CEAS Air&Space Conference, Venice, Italy, September 2011.

APPENDIX – SANDY3.0 SOFTWARE: GENERAL DESCRIPTION

SANDY is an in-house (currently not-commercial) code which has been developed and upgraded within last twenty-five years with the intent of providing an excellent and reliable tool for static and dynamic aeroelastic and aero-servo-elastic analysis of aircraft.

Rational approaches and validated numerical methods, compliant with EASA standards CS-25 and CS-23, have been implemented in a multidisciplinary computational environment able to accomplish the following main tasks:

- generation of A/C dynamic model (structural model and inertial model);
- generation of A/C aerodynamic model;
- generation of accurate transfer matrices interfacing between dynamic and aerodynamic models;
- evaluation of A/C acceleration and loads response due to flight and ground manoeuvre and/or gust;
- evaluation of A/C static and dynamic acceleration and loads response to movable lifting surfaces deflections imposed by mechanical and/or electro-mechanical control circuits;

https://doi.org/10.1017/S000192400000974X Published online by Cambridge University Press

- evaluation of divergence, control reversal and flutter speeds.

The computational tool, and the numerical methods within implemented, assure fast analyses aimed also to investigate the influence of several design parameters on A/C aeroelastic behaviour; in other terms, it is provided the capability of fast sensitivity aeroelastic analysis in correspondence of variations in structural and dynamic properties pertaining to A/C components including also the integrated control circuits.

The highly efficient computational structure is based on intercommunicating routines running in a common software environment (Visual Fortran®/Matlab®) and properly organised in three macro-modules:

- dynamic module;
- aerodynamic module;
- aeroelastic module.

The dynamic module includes a generator of A/C structural and inertial models as well as an internal FE solver for the evaluation of A/C modal parameters. In order to perform reliable modelling in reasonable time, only two typologies of elements are available:

- simple mono-dimensional elements (beam, rod, rigid-link, spring);
- DMIG (Direct Matrix Input at Grids) elements for a correct evaluation of stiffness and inertial properties of all those parts for which a mono-dimensional elements modelling leads to high approximations and/or is not applicable at all.

DMIG elements may also be imported by commercial FE software (e.g. MSC-NASTRAN®); the same applies to A/C modal parameters (modes shapes, frequencies, generalised masses, damping) which, moreover, may be imported directly from experimental data obtained by means of ground vibration tests.

In order to simulate loads alleviation systems based on movable surfaces in feed-back with A/C cinematic parameters (acceleration, velocity, displacements) and/or to perform fast instabilities analyses in presence of powered or fly-by-wire controls, the module is properly structured for the introduction of extra-modes representing movable surfaces deflections in addition to the normal modes related to A/C structure[4].

The aerodynamic module is characterised by a generator of aerodynamic model coupled to an internal solver for the evaluation of modal pressure distributions by means of consolidated numerical methods (e.g. Doublet Lattice Method). More in detail it is provided the capability of generating three-dimensional compressible aerodynamic models as well as the possibility of performing local corrections in pressure distributions in order to achieve a correct simulation of movable surfaces aerodynamics (as recommended by FAA AC 25.629-1A paragraph 6).

The aeroelastic module is finally constituted by all the routines devoted to:

- the interpolation of modal displacements on the aerodynamic lattice (matching routines implementing 3D spline methodologies);
- the evaluation of generalised aerodynamic pressures/forces and steady/unsteady aerodynamic influence coefficients;
- the solution of aeroelastic equations related to A/C aeroelastic response and aeroelastic instabilities identification.

Software overall facilities and performances have been positively tested during the certification processes of a wide set of commercial aircraft with reference to the aeroelastic stability demonstration at both theoretical and experimental levels (see as example (Ref. 22).

https://doi.org/10.1017/S000192400000974X Published online by Cambridge University Press